



Origin of abnormal glass transition behavior in metallic glasses



Weiming Yang^{a,b,c}, Jiawei Li^b, Haishun Liu^{a,*}, Chaochao Dun^d, Haolei Zhang^b,
Juntao Huo^b, Lin Xue^{a,b,c}, Yucheng Zhao^a, Baolong Shen^c, Linming Dou^a, Akihisa Inoue^{a,e}

^a State Key Laboratory for Geomechanics and Deep Underground Engineering, School of Mechanics and Civil Engineering, School of Sciences, State Key Laboratory of Coal Resources and Safe Mining, China University of Mining and Technology, Xuzhou 221116, China

^b Zhejiang Province Key Laboratory of Magnetic Materials and Application Technology, Key Laboratory of Magnetic Materials and Devices, Ningbo Institute of Materials Technology & Engineering, Chinese Academy of Sciences, Ningbo 315201, China

^c School of Materials Science and Engineering, Southeast University, Nanjing 211189, China

^d Department of Physics, Wake Forest University, Winston-Salem, NC 27109, USA

^e WPI Advanced Institute for Materials Research, Tohoku University, Sendai 980-8577, Japan

ARTICLE INFO

Article history:

Received 15 July 2013

Received in revised form

30 November 2013

Accepted 9 January 2014

Available online 31 January 2014

Keywords:

B. Glasses, metallic

D. Microstructure

ABSTRACT

In this paper, the phenomenon of two glass-transition-like appearance in the supercooled liquid region of metallic glasses was investigated. It is confirmed that this abnormal behavior is attributed to the transition process of an amorphous state from higher energy to lower energy. The amorphous state with higher energy comes from the uneven distribution of compositions in glasses, which is mainly caused by the component with significant differences in atomic size and nonnegative values of enthalpy of mixing. The results were verified by high resolution transmission electron microscopy and energy-dispersive spectrometry.

© 2014 Elsevier Ltd. All rights reserved.

1. Introduction

Metallic glasses (MGs) have attracted great attention due to their unique properties, such as ultrahigh strength [1], excellent soft magnetic properties [2,3], and good anticorrosion property [4] suitable in a wide range of applications [5–7]. As an important thermal property, glass transition has been a subject of much discussion since it plays an important role in the definition of MGs [8]. Moreover, the study of glass transition is also essential to explore the nature of glassy forming ability (GFA), thermodynamics, and intrinsic mechanism of glassy formation [9–11,12]. In general, the glass transition behavior during heating is characterized by a single endothermic reaction, i.e., the specific heat increases abruptly to a maximum value, and then remains constantly or slightly decreases down to crystallization onset temperature. Interestingly, two glass-transition-like appearance in supercooled liquid region (SLR) has been observed experimentally in various MGs [13–24]. Recently, many investigations revealed that the abnormal glass transition behavior is directly related to the high GFA and good plasticity of MGs [13,18,21]. Tanner et al. postulated that the abnormal behavior is originated from the phase separation [14]. However, no

experimental evidence was found supporting this mechanism [15]. Jiang et al. proposed that this abnormal behavior is strongly correlated to the local atomic structure reordering [19]. Park et al. further suggested that it should be originated from the growth reaction of quenched-in nuclei in the SLR [21,22]. These debates indicate that a physical understanding of the abnormal glass transition behavior in SLR is still unsettled.

In this letter, $(\text{Fe}_{0.71}\text{Dy}_{0.05}\text{B}_{0.24})_{96}\text{Nb}_4$ alloy was selected as a model glass to investigate the abnormal behavior of glass transition under uniaxial compression. Based on the concept that the deformation of MGs is actually the same response to the external energy (temperature or force) [25], the origin of abnormal glass transition behavior of MGs was studied systematically.

2. Experimental procedures

$(\text{Fe}_{0.71}\text{Dy}_{0.05}\text{B}_{0.24})_{96}\text{Nb}_4$ MG was prepared by arc melting the mixtures of Fe (99.99 mass %), Dy (99.99 mass %), Nb (99.99 mass %) metals and B (99.5 mass %) crystals in an argon atmosphere. Glassy ribbons and cylindrical rods with nominal compositions were prepared by a rapid quenching technology on a single copper wheel with a speed of 40 m/s and copper mold casting method, respectively. The structures of samples were identified by X-ray diffraction (XRD) with Cu $K\alpha$ radiation, high resolution transmission electron microscopy (HRTEM) and energy-dispersive spectrometry

* Corresponding author. Tel.: +86 139 12006872; fax: +86 516 83591591.
E-mail address: liuhaishun@126.com (H. Liu).

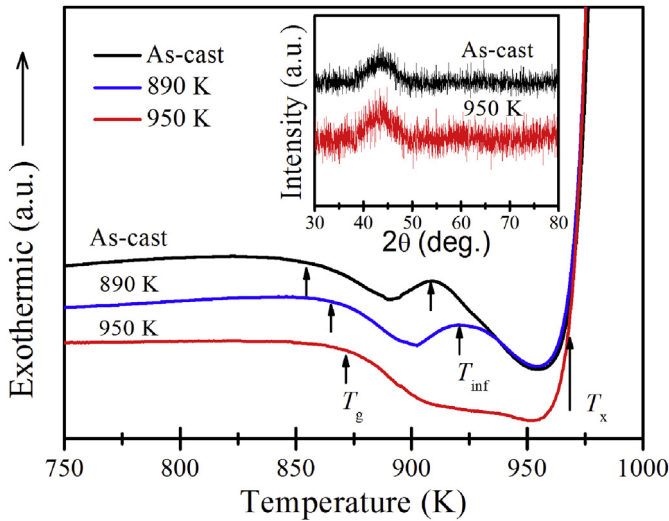


Fig. 1. DSC curves for as-quenched and annealed samples; the inset shows the XRD traces of the samples in as-quenched state and annealed at 950 K.

(EDS). The thermal stability of the glassy samples was examined using a NETZSCH 404 C differential scanning calorimeter (DSC) at a heating rate of 0.67 K/s under a flow of high purity argon. The glassy rods ($\Phi = 2$ mm) were cut to about 4 mm in length and their ends were carefully polished so as to be flat and parallel. The cylindrical rods were loaded for 5 min under each stress level of 2000, 3000, and 3500 MPa at room temperature by compression testing with an Instron testing machine with strain rate $5 \times 10^{-4} \text{ s}^{-1}$. The rods after uniaxial compression were re-examined by XRD and DSC. The density of samples in as-cast state and annealed state at 950 K for 0.5 h in vacuum was measured using Archimedes's method with the uncertainty less than 0.5%.

3. Results and discussion

Fig. 1 shows the XRD and DSC traces of specimens after annealing at different temperatures in SLR below the crystallization temperature (T_x). The XRD patterns of the as-quenched and annealed (at 950 K) samples display broad diffraction maxima, which is the characteristic of an amorphous structure. The sample annealed at 890 K shows a second inflection like the as-quenched samples. However, the second inflection of the annealed samples (at 950 K) almost disappears. Meanwhile, the glass transition temperature (T_g) increases from 860 K for the as-quenched sample to 875 K for that annealed at 950 K. The constant value of T_x after heating at different temperatures implies that there is no obvious progress in crystallization, which is in agreement with the XRD results. On the other hand, the slight rise in T_g suggests that the state of the amorphous phase changes during the heating through the second inflection temperature (T_{inf}).

Fig. 2 shows the XRD patterns of $(\text{Fe}_{0.71}\text{Dy}_{0.05}\text{B}_{0.24})_{96}\text{Nb}_4$ BMG in as-cast and compression states. No sharp Bragg peaks are detected for the compression samples, indicating that the glassy nature of these samples is quite stable at room temperature. However, with an increase of the compression pressure, the broad diffusive amorphous halo peak obviously shifts to a higher wave vector. According to the Bragg equation: $2r_1\sin\theta = \lambda$, the position of an X-ray halo maximum is directly related to the average radius of the first coordination shell r_1 , the X-ray wave length λ , and the scatter angle corresponding to the halo maximum 2θ . The shifts may indicate the changes of configuration coordination and topological rearrangements of atoms by compressing [26].

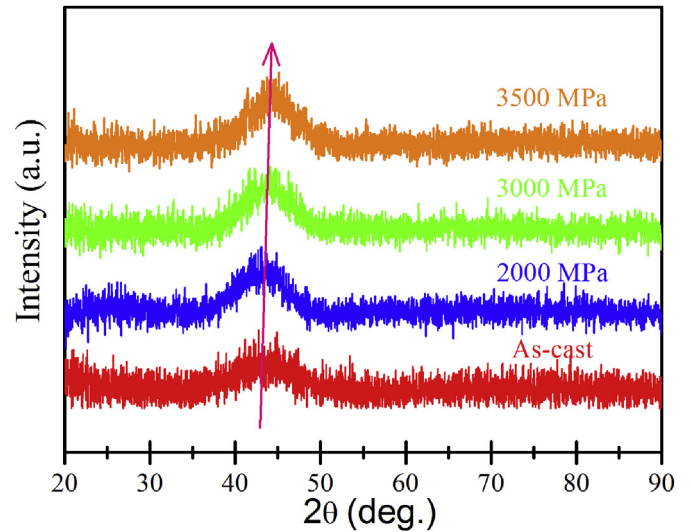


Fig. 2. XRD patterns of $(\text{Fe}_{0.71}\text{Dy}_{0.05}\text{B}_{0.24})_{96}\text{Nb}_4$ BMG in as-cast state and ones after compression.

Fig. 3 gives the DSC curves of $(\text{Fe}_{0.71}\text{Dy}_{0.05}\text{B}_{0.24})_{96}\text{Nb}_4$ MG in as-quenched ribbon, as well as as-cast and compressed rods. We can see that the exothermic event in the SLR is more noticeable for the ribbon than that for the rods. For the compressed rods, the amplitude of the first endothermic event decreases with the increasing pressure. The endothermic event ΔH were estimated to be -156.1 J/mol for ribbons, -89.4 J/mol for the uncompressed rod, -74.9 J/mol for the rod with 2000 MPa load, -71.6 J/mol for the rod with 3000 MPa load, and -64.0 J/mol for the rod with 3500 MPa load.

In glassy systems, the addition of elements with different atomic size and nonnegative values of enthalpy of mixing with others is likely to lead to a energy rise of the amorphous phase [27]. From the kinetic point of view [28], the energy barrier ΔG^* of the transition from one glassy state to another state at a given pressure P can be expressed by

$$\Delta G^*(T, P) = \frac{16\pi\gamma^3(V_m^{a_2})}{3[P(V_m^{a_1} - V_m^{a_2}) - (\Delta G^{a_1 \rightarrow a_2} + E_e)]^2} \quad (1)$$

where γ is the interfacial energy, $V_m^{a_1}$ and $V_m^{a_2}$ the molar volumes of the a_1 and a_2 glassy states, $\Delta G^{a_1 \rightarrow a_2}(T, P)$ the molar free energy change for the transformation from a_1 glassy state to a_2 glassy state, and E_e the elastic energy induced by the volume change during the transformation [29], which can be expressed as

$$E_e = \frac{E\varepsilon^2 V_m^{a_2}}{2} \quad (2)$$

where E is the Young's modulus and $\varepsilon = (V_m^{a_1} - V_m^{a_2})/3V_m^{a_2}$.

For $(\text{Fe}_{0.71}\text{Dy}_{0.05}\text{B}_{0.24})_{96}\text{Nb}_4$ MG, $E \approx 200$ GPa, $V_m^{a_2} = 6.94 \times 10^{-6} \text{ m}^3/\text{mol}$, and $V_m^{a_1} = 6.85 \times 10^{-6} \text{ m}^3/\text{mol}$. Therefore, the elastic strain energy is obtained as $E_e = 3014$ J/mol. Meanwhile, the interfacial energy γ of $(\text{Fe}_{0.71}\text{Dy}_{0.05}\text{B}_{0.24})_{96}\text{Nb}_4$ MG is about 1.5 J/m^2 [30,31]. Thus, the energy barrier ΔG^* can be calculated from Eq. (1) by setting the load to zero,

$$\Delta G^* = \frac{2.652 \times 10^{11}}{(\Delta G^{a_1 \rightarrow a_2} + 3014)^2} \text{ kJ/mol} \quad (3)$$

From Kissinger equation $\ln(\Phi/T_{inf}^2) = -E_a/RT_{inf} + C$ [32], here Φ is the heating rate, R the gas constant, C the constant, and E_a the overall activation energy for a_1 to a_2 glassy transformation at $P = 0$,

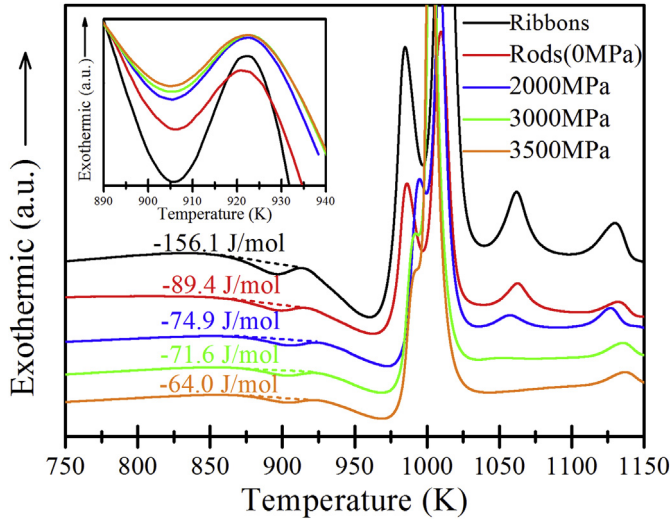


Fig. 3. DSC traces obtained for $(\text{Fe}_{0.71}\text{Dy}_{0.05}\text{B}_{0.24})_{96}\text{Nb}_4$ ribbons, also corresponding rods, uncompressed rods and compressed ones under 2000, 3000, and 3500 MPa. The inset shows the magnified figure of the first inflection curves in the SLR.

which is determined to be about 102.3 kJ/mol, as shown in Fig. 4. Here, E_a can be also estimated as [33]

$$E_a = \frac{\Delta G^* + m\Delta E_d}{n} = 102.3 \text{ kJ/mol} \quad (4)$$

where ΔE_d is the diffusion energy barrier in Fe-based MGs, which is around 95.4 kJ/mol (1.0 eV) [33]. The values of n and m are 4 and 3, respectively [34]. Then, the energy barrier ΔG^* of the glassy alloy is determined as 123 kJ/mol. Therefore, we obtain that $\Delta G^{a_1 \rightarrow a_2}$ is -49.447 kJ/mol from Eq. (3). Substituting the corresponding values of γ , $V_m^{a_2}$, $V_m^{a_1}$, $\Delta G^{a_1 \rightarrow a_2}$ and E_e into Eq. (1), the relationship between the energy barrier and uniaxial pressure can be drawn as

$$\Delta G^*(P) = \frac{2.652 \times 10^{11}}{(90P + 46433)^2} \text{ kJ/mol} \quad (5)$$

Fig. 5(a) shows the calculation results about how uniaxial load influences the energy barrier according to Eq. (5). At the same time,

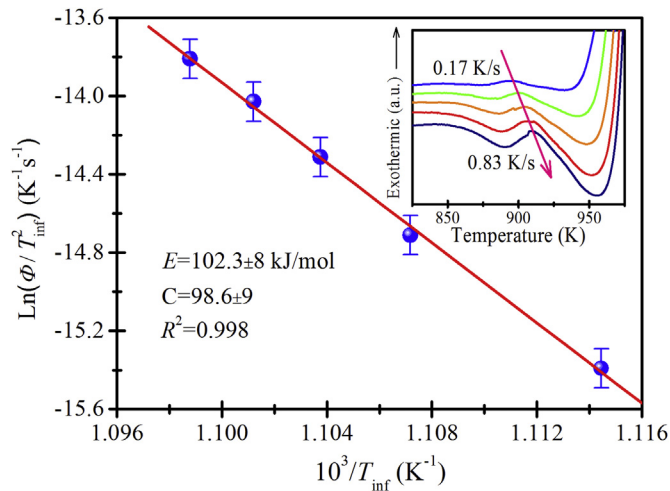


Fig. 4. Kissinger plot for the $(\text{Fe}_{0.71}\text{Dy}_{0.05}\text{B}_{0.24})_{96}\text{Nb}_4$ MG. The fitting linear in red shows a correlation parameter of $R^2 = 0.998$. The inset is the enlarged DSC curves in SLR at variable heating rates from 0.17 to 0.83 K/s. The peak temperature T_{inf} in SLR is indicated for activation energy calculations.

the energy barrier of glassy transitions can be effectively reduced by compression load, as shown in Fig. 5(b).

From the above analysis, we can conclude that the abnormal glass transition behavior is attributed to the transition process of an amorphous state from a higher energy state to a lower one. To further interpret this phenomenon, a more general version of discuss is presented in Fig. 6. From Fig. 6, we can see that the formation of MGs is the competition process between supercooling liquid phase and crystallization [35,36], which is strongly associated with the radius and enthalpy of mixing of each atom pair [37]. The components with significant difference in atomic size and enthalpy of mixing will cause either the local aggregation or dispersion of elements, which results in the uneven structure of glasses [38]. Accompanied by the uneven distribution of compositions, the composition in these local regions deviates from the statistic average of the compositions, which leads to the generational heterogeneous structure regions in the glasses. In analogy with the internal stress, the heterogeneous structure lies in a higher energy state, which is unstable even a certain energy barrier exists. Under certain annealing conditions, heat will be released in the transition process from glassy state with higher energy to the one with a lower energy, resulting in the formation of peak in the SLR. The external force can effectively reduce the energy barrier so that the absorbed heat needed for triggering the transformation will be cut down, which is the exact reason to the relatively shallow valley value in the DSC curve. Besides, the pressure load introduced by the

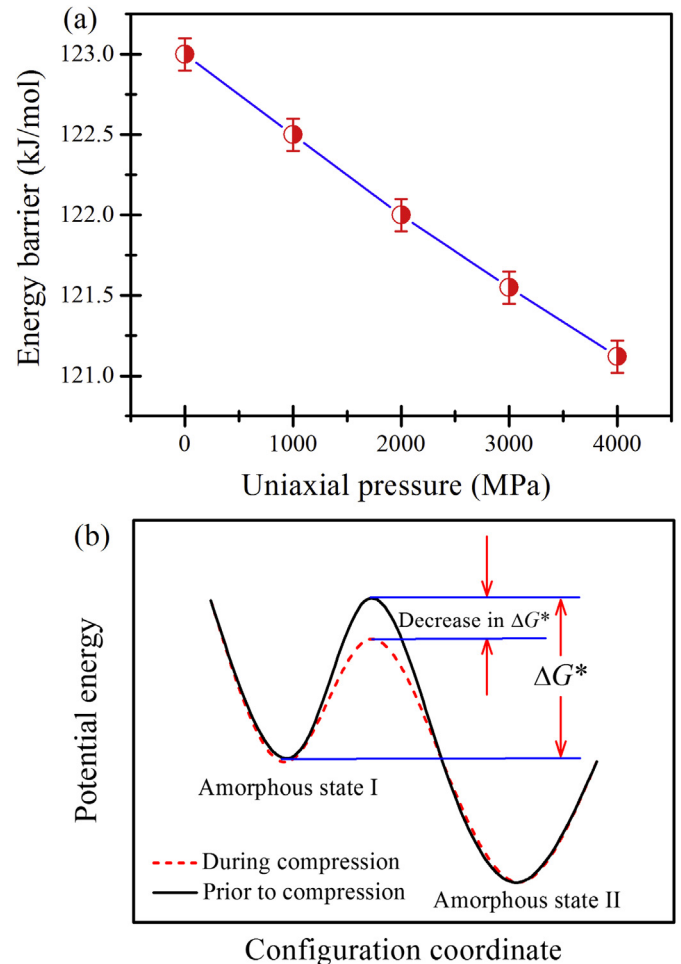


Fig. 5. (a) The uniaxial pressure dependence of energy barrier. (b) Schematic diagram of the relative energy states of glasses before and during uniaxial compression.

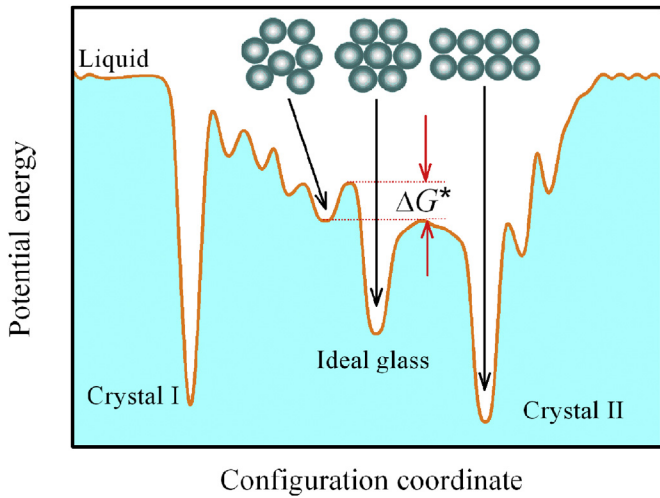


Fig. 6. Schematic illustration of possible thermodynamic states of glasses.

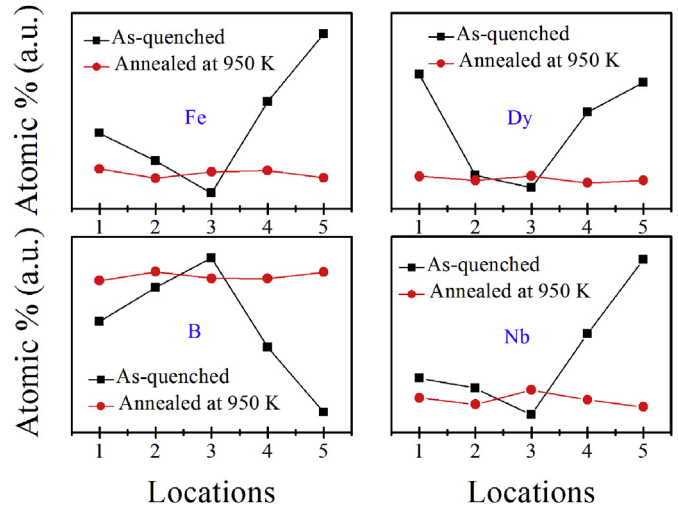


Fig. 9. EDS measured atomic compositions of five randomly selected areas in the as-quenched samples and the ones annealed at 950 K, respectively.

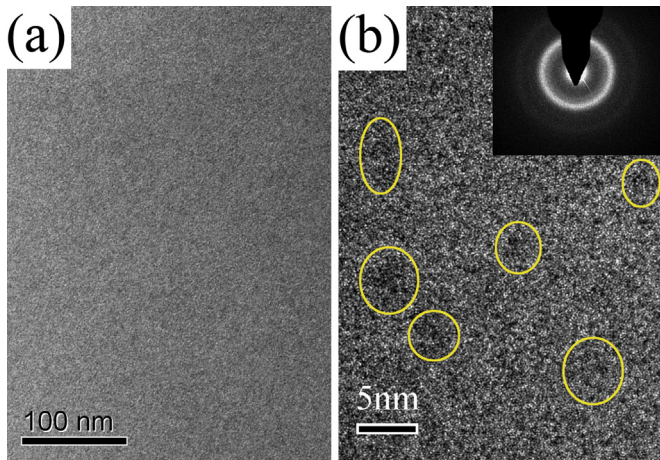


Fig. 7. (a) Low-magnification TEM, (b) HRTEM images and their corresponding SAED patterns of the samples in as-quenched state.

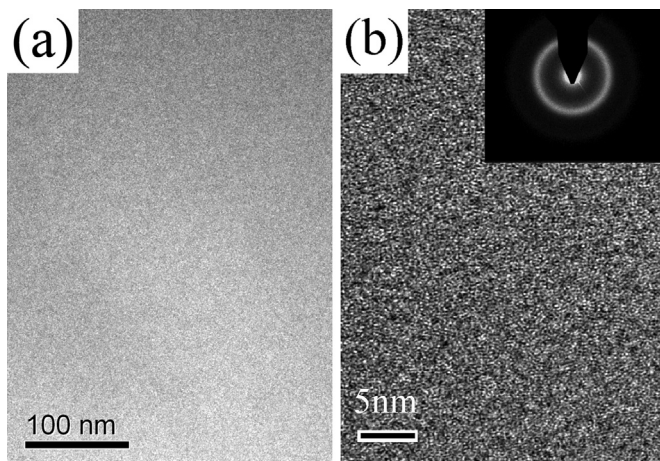


Fig. 8. (a) Low-magnification TEM, (b) HRTEM images and their corresponding SAED patterns of the samples after annealed at 950 K.

external force has the ability to decrease the distance between constituent atoms, change the atomic configurations, and finally affect the exothermic/endothermic conditions to some extent for the alloys subjected to compression.

In order to confirm the described analysis, HRTEM images and their corresponding selected area electron diffraction (SAED) patterns of the as-quenched and annealed at 950 K samples are shown in Figs. 7 and 8, respectively. No crystalline phase is observed. The inserted SAED patterns exhibit a single diffraction halo, with no sharp diffraction rings observed. It is thus confirmed that each sample possess a fully glassy structure. More importantly, there is a slight difference between Fig. 7(b) and Fig. 8(b), which is marked with circles in Fig. 7(b) that represents the locally inhomogeneous regions. We also measured the atomic compositions for the randomly selected areas by semi-quantitative EDS, as shown in Fig. 9. It indicates that there are detectable fluctuations in the local chemical compositions in the as-quenched samples, whereas nearly no fluctuation exists in samples annealed at 950 K. These results further reveal that the abnormal behavior of glass transition comes from the structural heterogeneity in the as-cast $(\text{Fe}_{0.71}\text{Dy}_{0.05}\text{B}_{0.24})_{96}\text{Nb}_4$ MG. The relationship between the abnormal glass transition behavior and the structural heterogeneity by the addition of an element for other existing MGs were also summarized in Table 1. All the additional elements have significant differences in atomic size and nonnegative mixing enthalpy with respect to the parent elements, which can result in the local aggregation or dispersion of elements (structural heterogeneity), then the abnormal glass transition behavior as we discussed.

4. Conclusion

In this paper, the origin of the abnormal behavior in the SLR was investigated by measuring the changes in DSC curves, X-ray diffraction patterns, and HRTEM images of uniaxial compression. It is shown that this phenomenon arises from the increase of unstable atomic scale heterogeneity, which is mainly caused by the components with significant differences in atomic size and nonnegative values of enthalpy of mixing. Considering the strong correlation among the heterogeneity, plasticity and GFA, this result assists in the design of novel MGs with both high GFA and large ductility.

Table 1
Thermal properties of T_g , T_{inf} , T_x , r_{max}/r_{min} (the subscript “max” and “min” denotes the elements with maximum and minimum atomic radius in the compositions, respectively) and ΔH_{A-B} (the nonnegative enthalpy of mixing for different atomic pairs in these MG systems) for a fully amorphous state in MGs with abnormal behavior in SLR.

Metallic glasses	T_g (K)	T_{inf} (K)	T_x (K)	r_{max}/r_{min} ^a	ΔH_{A-B} ^b (kJ/mol)	References
(Fe _{0.72} Dy _{0.03} B _{0.2} Si _{0.05}) ₉₆ Nb ₄	860	910	940	2.06	$\Delta H_{Nb-Dy} = +27$	[13]
Zr ₃₆ Ti ₂₄ Be ₄₀	628	663	713	1.44	$\Delta H_{Zr-Ti} = 0$	[14,15]
Pd _{40.5} Ni _{40.5} P ₁₉	576	623, 638	653	1.27	$\Delta H_{Pd-Ni} = 0$	[16,17]
(Fe _{0.72} B _{0.24} Nb _{0.04}) _{95.5} Y _{4.5}	871	925	982	2.09	$\Delta H_{Nb-Y} = +30$	[18]
Fe ₆₈ Nb ₄ Y ₆ B ₂₂	880	915	933	2.09	$\Delta H_{Nb-Y} = +30$	[19]
Ni ₆₁ Zr ₂₂ Nb ₇ Al ₄ Ta ₆	876	879	934	1.29	$\Delta H_{Zr-Nb} = +15$	[20]
Cu ₄₆ Zr ₄₂ Al ₇ Y ₅	680	739	771	1.44	$\Delta H_{Zr-Y} = +35$	[21]
Mg ₆₅ Cu ₁₅ Ag ₁₀ Gd ₁₀	416	443	459	1.44	$\Delta H_{Cu-Ag} = +5$	[21]
Cu ₄₃ Zr ₄₃ Ag ₇ Y ₃ Al ₇	710	743, 775	790	1.44	$\Delta H_{Zr-Y} = +35$	[21]
Cu ₅₅ Zr ₄₀ Sn ₅	757	775	792	1.28	$\Delta H_{Cu-Sn} = +7$	[22]
(Fe _{0.9} Co _{0.1}) _{67.5} Nb ₄ Gd _{3.5} B ₂₅	850	910	960	2.10	$\Delta H_{Nb-Gd} = +30$	[23]
Nd ₃ Y ₃ Fe ₆₈ Mo ₄ B ₂₂	870	900	970	2.11	$\Delta H_{Nd-Mo} = +26$	[24]

^a Reference [39].

^b Reference [40].

Acknowledgments

We are indebted to Dr. Diana Estévez for constructive and valuable suggestions on our paper. This work was supported by the National Natural Science Foundation of China (Grant No. 51074155, 50825103, 51271194, and 50834004) and National Basic Research Program of China (2010CB226805).

References

- [1] Inoue A, Shen BL, Koshiba H, Kato H, Yavari AR. *Nat Mater* 2003;2:661.
- [2] Jiao ZB, Li HX, Gao JE, Wu Y, Lu ZP. *Intermetallics* 2011;19:1502.
- [3] Yang WM, Liu HS, Xue L, Li JW, Dun CC, Zhang JH, et al. *J Magn Magn Mater* 2013;335:172.
- [4] Pang SJ, Zhang T, Asami K, Inoue A. *Acta Mater* 2002;50:489.
- [5] Fujita K, Zhang W, Shen BL, Amiya K, Ma CL, Nishiyama N. *Intermetallics* 2012;30:12.
- [6] Wang JQ, Liu YH, Chen MW, Xie GQ, Louzguine-Luzgin DV, Inoue A, et al. *Adv Func Mater* 2012;22:2567.
- [7] Inoue A, Shen BL, Takeuchi A. *Mater Sci Eng A* 2006;441:18.
- [8] Anderson PW. *Science* 1995;267:1615.
- [9] Lu ZP, Liu CT. *Acta Mater* 2002;50:3501.
- [10] Egami T, Poon SJ, Zhang Z, Keppens V. *Phys Rev B* 2007;76:024203.
- [11] Debenedetti PG, Stillinger FH. *Nature* 2001;410:259.
- [12] Ke HB, Wen P, Wang WH. *AIP Adv* 2012;2:041404.
- [13] Li JW, Yang WM, Zhang MX, Chen GX, Shen BL. *J Non Cryst Solids* 2013;365:42.
- [14] Tanner LE, Ray R. *Scr Mater* 1980;14:657.
- [15] Kumar G, Nagahama D, Ohnuma M, Ohkubo T, Hono K. *Scr Mater* 2006;54:801.
- [16] Madge SV, Rösner H, Wilde G. *Scr Mater* 2005;53:1147.
- [17] Li Y, Qiu SB, Yang S, Yao KF. *Chin Phys Lett* 2011;28:116104.
- [18] Lee S, Kato H, Kubota T, Yubuta K, Makino A, Inoue A. *Mater Trans* 2008;49:506.
- [19] Huang XM, Wang XD, He Y, Cao QP, Jiang JZ. *Scr Mater* 2009;60:152.
- [20] Na JH, Sohn SW, Kim WT, Kim DH. *Scr Mater* 2007;57:225.
- [21] Park ES, Na JH, Kim DH. *J Appl Phys* 2010;108:053515.
- [22] Park ES, Ohnuma M, Kim DH. *J Alloys Compd* 2011;509S:S52.
- [23] Zhang W, Jia F, Zhang XG, Xie GQ, Inoue A. *Metall Mater Trans A* 2010;41A:1685.
- [24] Wu Q, Yan AR, Ge HL, Zhang PY, Hu XK, Liu YH. *J Appl Phys* 2011;109:07A739.
- [25] Wang WH. *J Appl Phys* 2011;110:053521.
- [26] Lou HB, Wang XD, Cao QP, Zhang DX, Zhang J, Hu TD, et al. *Proc Natl Acad Sci U S A* 2013;110:10068.
- [27] Park ES, Chang HJ, Lee JY, Kim DH. *J Mater Res* 2007;22:3440.
- [28] Zhuang YX, Jiang JZ, Zhou TJ, Rasmussen H, Gerward L, Mezouar M, et al. *Appl Phys Lett* 2000;77:4133.
- [29] Inoue A, Kimura HM, Sasamori K, Masumoto T. *Sci Rep Res Inst Tohoku Univ A* 1996;42:165.
- [30] Iida T, Guthrie RIL. *The physical properties of liquid metals*. Oxford: Clarendon; 1988. p. 134.
- [31] Yuan CC, Xi XK. *J Appl Phys* 2011;109:033515.
- [32] Kissinger HE. *J Res Natl Bur Stand Sect A* 1956;57:217.
- [33] Jiang HG, Ding BZ, Wang JT. *Acta Metal Sin* 1992;28:B27.
- [34] Yinnon H, Uhlmann DR. *J Non Cryst Solids* 1983;54:253.
- [35] Lu ZP, Liu CT. *Phys Rev Lett* 2003;91:115505.
- [36] Fujita T, Konno K, Zhang W, Kumar V, Matsuura M, Inoue A, et al. *Phys Rev Lett* 2009;103:075502.
- [37] Inoue A. *Acta Mater* 2000;48:279.
- [38] Zheng N, Qu RT, Pauly S, Calin M, Gemming T, Zhang ZF, et al. *Appl Phys Lett* 2012;100:141901.
- [39] Speight JG. *Lang's handbook of chemistry*. 16th ed. London: Mc Graw-Hill; 2005.151.
- [40] Takeuchi A, Inoue A. *Mater Trans* 2005;46:2817.